Fault Detection and Exclusion for INS/GPS/5G Tightly-Coupled Navigation

Mu Jia and Zaher M. Kassas

Department of Electrical and Computer Engineering
The Ohio State University, Columbus, OH, USA
`jia.641@osu.edu, zkassas@ieee.org`

Abstract—A solution separation-based fault detection and exclusion (FDE) framework is developed for GPS and 5G signal of opportunity (SOP) aided inertial navigation system (INS). The proposed framework fuses an inertial measurement unit (IMU) with GPS and 5G pseudorange measurements in a tightly-coupled fashion via an extended Kalman filter to estimate the ground vehicles' attitude, position, velocity, and clock errors. Solution separation tests are exploited to detect and exclude faults from GPS and 5G signals due to transmitter failures and local threats in urban environments (e.g., multipath). Experimental results are presented to evaluate the efficacy of the proposed framework under different sensor fusion scenarios. It is shown that fusing 5G signals enhances the FDE performance of the multi-sensor system in a suburban scenario: while INS/GPS fails to detect faulty GPS measurements, the INS/GPS/SOP is able to detect the fault. Moreover, over a trajectory of 1.91 km traversed in 200 s, using signals from two 5G gNBs, the INS/GPS/5G system achieved a position root-mean squared error (RMSE) of 0.81 m and maximum position error of 2.17 m. The undetected GPS fault in the INS/GPS system increased the RMSE and maximum position error to 1.83 m and 4.25 m, respectively.

Index Terms—opportunistic navigation, RAIM, fault detection, solution separation, 5G.

I. INTRODUCTION

The world is fast approaching an era of autonomous driving, which is powered by recent developments in artificial intelligence (AI), computing, communication as well high-precision navigation technologies. However, ensuring safety of the automated driving function is one of the most significant obstacles facing the development, commercialization, and adoption of fully-automated vehicles. Analysis of reported accidents that involved automated vehicles indicate that most of the wrong decisions from the self-driving system are triggered by failures in the positioning, navigation, and perception system [1].

Ground vehicle navigation systems utilize global navigation satellite system (GNSS) receivers and a suite of onboard sensors, e.g., lidar, camera, radar, inertial navigation system (INS), etc. GNSS receivers are relied upon to provide a navigation solution in a global frame and to correct for accumulating errors due to the bias and drift of sensor dead reckoning. While achieving higher levels of navigation accuracy has been a classic requirement, the trustworthiness in the navigation

solution, commonly assessed by integrity measures, as well as the ability of fault detection and exclusion (FDE) is evermore vital in the safety-critical application of automated driving. To ensure safe navigation, automated vehicles need to instantaneously detect receiver and sensor failures and have the capability of excluding possible faults to maintain continuous high-integrity navigation.

Current GNSS technologies are insufficient to support the transition of ground vehicles to full automation in terms of accuracy, integrity, and availability [2]. While analysis indicates that driverless vehicles will need centimeter-level navigation accuracy on local and residential streets [3], single point positioning (SPP) can only achieve meter-level accuracy [4]. Integration of GNSS receivers with an INS improves the navigation solution by taking advantage of the short-term accuracy of the INS, coupled with the long-term stability of the GNSS solution. However, sub-meter-level accuracy is achievable with certain augmentation systems and real-time kinematic (RTK) only under certain favorable conditions [5]. In terms of integrity and availability, recent work demonstrated that in a sample downtown environment (Chicago urban corridor), availability of GPS-only positioning was less than 10% at most locations. While integration of multi-constellation GNSS, INS, wheel speed sensors, zero velocity updates, and vehicle kinematic constraint improved the availability significantly, it was still challenging to maintain availability after the vehicle traversed 4,500 m in an urban environment [6].

Recently, signals of opportunity (SOPs) [7]; e.g., cellular signals [8]–[11], digital television [12], and FM [13]; have been been demonstrated as an attractive alternative or supplement to GNSS signals. For vehicular navigation in urban environments [14]–[16], cellular SOPs are particularly attractive due to their inherent attributes: abundance, geometric and spectral diversity, high received power, and large bandwidth. With the fast deployment of fifth-generation (5G) cellular systems, their navigation capabilities have attracted extensive research efforts [17]–[22]. Recent literature exploited downlink 5G signals and showed favorable positioning accuracy [23], [24].

Integrity monitoring of multi-sensor integrated navigation has attracted research efforts during the last couple of decades [25]. Receiver autonomous integrity monitoring (RAIM), which was initially introduced in aviation, has been adapted to account for multi-constellation GNSS measurements [26]

(e.g., Galileo [27], GLONASS [28], and Beidou [29]), aiding sensors (e.g., INS-GPS [30], lidar-GNSS [31], vision-GPS [32], and multi-sensor collaborative [33]), and terrestrial SOPs [34]–[36]. As tightly-coupled GNSS/INS is widely adopted for vehicular navigation, different integrity monitoring frameworks have been proposed, e.g., extended RAIM [37], solution separation [38], residual-based method [39], and innovation-based method [40]. Initial studies to characterize the integrity monitoring improvement for automated driving, upon fusing GPS signals with terrestrial SOPs, was conducted in [41], [42]. However, the research on FDE for opportunistic navigation, especially for SOP-aided inertial navigation is rarely found in the literature. An extended Kalman filter (EKF)-based solution separation RAIM, which fuses sequential GNSS and SOP measurements was proposed in [43]. Nevertheless, a simple vehicle dynamics models was adopted and no fault exclusion results were presented. This paper extends the previous work by incorporating an INS and developing the FDE algorithm. To this end, a solution separation-based FDE framework is developed for INS/GPS/5G. Solution separation tests are exploited to detect and exclude faults from GPS and 5G signals due to transmitter failures and local threats in urban environments (e.g., multipath). Experimental results are presented to evaluate the efficacy of the proposed framework under different sensor fusion scenarios. It is shown that fusing 5G signals enhances the FDE performance of the multi-sensor system in a suburban scenario: while INS/GPS fails to detect faulty GPS measurements, the INS/GPS/SOP is able to detect the fault. Moreover, over a trajectory of 1.91 km traversed in 200 s, using signals from two 5G gNBs, the INS/GPS/5G system achieved a position root-mean squared error (RMSE) of 0.81 m and maximum position error of 2.17 m. The undetected GPS fault in the INS/GPS system increased the RMSE and maximum position error to 1.83 m and 4.25 m, respectively.

The rest of the paper is organized as follows. Section II introduces navigation models for GPS/SOP-aided INS. Section III describes the proposed integrity monitoring framework. Section IV presents the experiment results in a suburban environment and compares the FDE performance of different sensor fusion scenarios. Section V concludes the paper.

II. GPS/SOP-Aided Inertial Navigation

This section describes foundational models for the INS/GPS/SOP tightly coupled navigation framework, including the GPS and terrestrial SOP pseudorange measurement models, the aided INS states, the dynamics of the vehicle-mounted receiver and cellular SOP clocks, and the EKF-based navigation framework.

A. GPS Pseudorange Measurement Model

The ground vehicle is equipped with a receiver which makes pseudorange measurements to M GPS satellites. Let $\boldsymbol{z}^{\mathrm{G}}(k)$ denote the GPS measurement vector at time-step k defined as

$$\boldsymbol{z}^{\mathrm{G}}(k) = [z_1^{\mathrm{G}}(k), \ldots, z_m^{\mathrm{G}}(k), \ldots, z_M^{\mathrm{G}}(k)]^{\mathsf{T}},$$

where $z_m^{\mathrm{G}}(k)$ is the m-th GPS pseudorange measurement at time-step k, after compensating for ionospheric and tropospheric delays and satellite's clock bias, which is modeled as

$$z_m^{\mathrm{G}}(k) = \|\boldsymbol{r}_r(k) - \boldsymbol{r}_m^{\mathrm{G}}(k)\|_2 + c \cdot \delta t_r(k) + v_m^{\mathrm{G}}(k), \quad (1)$$

where $\boldsymbol{r}_r(k)$ and $\boldsymbol{r}_m^{\mathrm{G}}(k)$ are the receiver and m-th satellite's three-dimensional (3–D) position vectors, respectively; c is the speed of light; $\delta t_r(k)$ is the GPS receiver's clock bias; and v_m^{G} is the measurement noise, which is modeled as a zero-mean white Gaussian sequence with variance $(\sigma_m^{\mathrm{G}})^2(k)$.

B. Terrestrial SOP Pseudorange Measurement Model

The ground vehicle-mounted receiver also makes pseudorange measurements from N terrestrial SOPs, which are assumed to be stationary with known positions. Let $\boldsymbol{z}^{\mathrm{S}}(k)$ denote the SOP measurement vector at time-step k, defined as

$$\boldsymbol{z}^{\mathrm{S}}(k) = [z_1^{\mathrm{S}}(k), \ldots, z_n^{\mathrm{S}}(k), \ldots, z_N^{\mathrm{S}}(k)]^{\mathsf{T}},$$

where $z_n^{\mathrm{S}}(k)$ is the n-th SOP measurement at time-step k, which can be modeled as

$$z_n^{\mathrm{S}}(k) = \|\boldsymbol{r}_r(k) - \boldsymbol{r}_n^{\mathrm{S}}\|_2 + c \cdot [\delta t_r^{\mathrm{S}}(k) - \delta t_n^{\mathrm{S}}(k)] + v_n^{\mathrm{S}}(k), \quad (2)$$

where $\boldsymbol{r}_n^{\mathrm{S}}$ and $\delta t_n^{\mathrm{S}}(k)$ are the 3–D position and clock bias of the n-th SOP transmitter, respectively; $\delta t_r^{\mathrm{S}}(k)$ is the the receiver's clock bias (assumed to be different than the GPS receiver's clock bias $\delta t_r(k)$); and $v_n^{\mathrm{S}}(k)$ is the measurement noise, which is modeled as a zero-mean white Gaussian sequence with variance $(\sigma_n^{\mathrm{S}})^2(k)$.

C. Aided INS

The vehicle-mounted IMU produces 3–D angular velocity measurements $\boldsymbol{\omega}_{imu}(k)$ and specific force measurements $\boldsymbol{a}_{imu}$. An EKF is used to fuse IMU, GPS, and 5G SOP measurements [44]. The EKF state vector is defined as

$$\boldsymbol{x} \triangleq [{}_e^b\boldsymbol{q}^{\mathsf{T}}, \boldsymbol{r}_r^{\mathsf{T}}, \dot{\boldsymbol{r}}_r^{\mathsf{T}}, \boldsymbol{b}_{gyr}^{\mathsf{T}}, \boldsymbol{b}_{acc}^{\mathsf{T}}, \boldsymbol{x}_{\mathrm{clk},r}^{\mathsf{T}}, \boldsymbol{x}_{\mathrm{clk}}^{\mathrm{S}}{}^{\mathsf{T}}]^{\mathsf{T}}, \quad (3)$$

where ${}_e^b\boldsymbol{q}$ is the 4–D unit quaternion, representing the vehicle's orientation, i.e., rotation from Earth-centered, Earth-fixed (ECEF) frame {e} to vehicle body frame {b}, $\dot{\boldsymbol{r}}_r$ is the vehicle's speed, $\boldsymbol{b}_{gyr}$ is the gyroscope's 3–D bias, $\boldsymbol{b}_{acc}$ is the accelerometer's 3–D bias, $\boldsymbol{x}_{\mathrm{clk},r} = [\delta t_r, \dot{\delta t}_r]^{\mathsf{T}}$ is the GPS receiver clock error state vector, with $\dot{\delta t}_r$ denoting the receiver clock drift; and $\boldsymbol{x}_{\mathrm{clk}}^{\mathrm{S}}$ captures the difference between the SOP receiver and each of the SOPs' transmitters clock errors.

The discrete-time dynamics of $\boldsymbol{x}_{\mathrm{clk},r}$ and $\boldsymbol{x}_{\mathrm{clk}}^{\mathrm{S}}$ is assumed to follow the standard double integrator model, driven by process noise [44].

The time-update of ${}_e^b\boldsymbol{q}$, $\boldsymbol{r}_r$, and $\dot{\boldsymbol{r}}_r$ are performed using ECEF strapdown mechanization equations with the gyroscope and accelerometer measurements [45]. The EKF measurement-update corrects the time-updated states $\hat{\boldsymbol{x}}(k+1|k)$ using available GPS and SOP pseudorange measurements. The EKF measurement-updated states $\hat{\boldsymbol{x}}(k+1|k+1)$ and associated estimation error covariance $\mathbf{P}(k+1|k+1)$ are computed using standard EKF update equations [44].

III. Solution Separation-Based RAIM with FDE

This section describes the solution separation-based RAIM for aided INS, which fuses measurements from IMU, GPS, and SOPs, to detect and exclude faults from GPS and SOP measurements. Note that the proposed frameworks assume no fault condition in IMU measurements.

A. Framework Overview

As shown in Fig. 1, the proposed aided INS RAIM framework extends the framework developed in [43] by incorporating INS and fault detection functionality. The integrity monitoring system utilizes a bank of filters, upon which solution separation tests are conducted to detect potential faults from the ranging measurement, while assuming the INS is faultless. When faults are detected, exclusions are tried to resume normal operation.

B. Solution Separation Test

The test statistics are chosen to be the difference between the position estimates from the main filter, $\hat{r}^{(0)}(k|k)$, and the position estimates from the subfilters, $\hat{r}^{(i)}(k|k)$ [43]. The test statistics vector can be expressed as

$$\boldsymbol{x}_{ss}^{(i)}(k) = \hat{\boldsymbol{r}}^{(0)}(k|k) - \hat{\boldsymbol{r}}^{(i)}(k|k), \qquad i = 1, \ldots, N_{ss}, \quad (4)$$

where N_{ss} is the number of subfilters, i.e., the number of faulted hypotheses to be monitored.

As shown in [46], the covariance of the i-th solution separation vector can be computed as

$$\boldsymbol{\Sigma}_{ss}^{(i)}(k) = \mathbf{P}^{(i)}(k|k) - \mathbf{P}^{(0)}(k|k). \quad (5)$$

This enables the framework to calculate $\boldsymbol{\Sigma}_{ss}^{(i)}$ without having the cross-correlation between the main filter and subfilters.

The test threshold for the i-th hypothesis in the q-th direction is set to meet a predefined probability of false alert P_{fa} under nominal conditions according to

$$T_{i,q} = Q^{-1}(\alpha_{i,q} P_{fa}) \sigma_{ss,q}^{(i)}, \quad (6)$$

where $Q^{-1}(\cdot)$ is the inverse Q-function, $\alpha_{i,q}$ is the allocation coefficients of the false alert budget to q direction of the i-th fault mode, and $\sigma_{ss,q}^{(i)}$ is the q-th diagonal element of $\boldsymbol{\Sigma}_{ss}^{(i)}$.

C. FDE and Filter Management

After each time-step, when the system receives new pseudorange measurements, the test statistics of all subsets on all three directions are compared with their corresponding test thresholds. The system will be determined as in normal operation if all the tests pass, i.e.,

$$x_{ss,q}^{(i)} < T_{i,q}, \qquad i = 1, \ldots, N_{ss}, q = 1, 2, 3. \quad (7)$$

Otherwise, if any of the above tests fails, the system is deemed as in faulty conditions and the fault exclusion algorithm tries to recover the system by excluding the measurements associated with the failed tests.

The fault exclusion algorithm consists of reconstructing the filters and recalculating the estimation solutions. For example,

if any of the three tests for the i-th subset fails at time-step k_d, the subsets will be reconstructed based on the measurements excluding the ones associated with the i-th subset. The new subsets will be reinitialized based on the estimation solution from the main filter at time-step $k_d - k_{con}$, where k_{con} is a design parameter to allow the reconstructed subsets to converge. The reconstructed subsets will be propagated from time $k_d - k_{con}$ to the current time k_d. The purpos of the recalculation is twofold: (i) to rule out the possibility that the faulty measurements have contaminated the navigation solution before time-step k, and (ii) to recover the convergence of the reconstructed subfilter, so that the system can resume normal operation immediately, rather than waiting for future measurements until the filters converge. If the new subsets pass all the solution separation tests at time-step k_d, the system resume to normal operation with the remaining measurements after the exclusion. Otherwise, an alarm will be raised, as no possible exclusion is available. Algorithm 1 summarizes the FDE and filter management calcululations.

Algorithm 1 FDE and filter management

Input: N_{ss}, k, k_{con}, $\{\hat{\boldsymbol{x}}^{(0)}(j|j)\}_{j=1}^{k}$, $\{\mathbf{P}^{(0)}(j|j)\}_{j=1}^{k}$, $\{\hat{\boldsymbol{x}}^{(i)}(k|k)\}_{i=0}^{N_{ss}}$, $\{\mathbf{P}^{(i)}(k|k)\}_{i=0}^{N_{ss}}$, $\{\boldsymbol{z}(j)\}_{j=1}^{k}$, $\{\boldsymbol{\omega}_{imu}(j)\}_{j=1}^{k}$, $\{\boldsymbol{a}_{imu}(j)\}_{j=1}^{k}$

Output: $\{\hat{\boldsymbol{x}}^{(i)}(k|k)\}_{i=0}^{N_{ss}}$, $\{\mathbf{P}^{(i)}(k|k)\}_{i=0}^{N_{ss}}$

1:   $f \leftarrow 0$
2:   **for** $i \in \{1, \ldots, N_{ss}\}$ **do**
3:       **if** any test (6) fails for $\hat{\boldsymbol{x}}^{(i)}(k|k)$ **then**
4:          $f \leftarrow i$
5:          **break**
6:       **end if**
7:   **end for**
8:   **if** $f \neq 0$ **then**
9:       $\{\boldsymbol{z}_e(j)\}_{j=1}^{k} \leftarrow \{\boldsymbol{z}(j)\}_{j=1}^{k}$ excluding $\{z_f(j)\}_{j=1}^{k}$
10:     $k_e \leftarrow k - k_{con}$
11:     Reconstruct subsets at k_e
12:     Initialize $\{\hat{\boldsymbol{x}}_e^{(i)}(k_e|k_e)\}_{i=0}^{N_{ss}-1}$, $\{\mathbf{P}_e^{(i)}(k_e|k_e)\}_{i=0}^{N_{ss}-1}$ with corresponding element from $\hat{\boldsymbol{x}}^{(0)}(k_e|k_e)$, $\mathbf{P}^{(0)}(k_e|k_e)$
13:     Propagate filters to calculate $\{\hat{\boldsymbol{x}}_e^{(i)}(k|k)\}_{i=0}^{N_{ss}-1}$, $\{\mathbf{P}_e^{(i)}(k|k)\}_{i=0}^{N_{ss}-1}$
14:     **for** $i \in \{1, \ldots, N_{ss} - 1\}$ **do**
15:       **if** any test (6) fails for $\hat{\boldsymbol{x}}_e^{(i)}(k|k)$ **then**
16:          **Return** Fault with no exclusion
17:       **end if**
18:     **end for**
19:     $\{\hat{\boldsymbol{x}}^{(i)}(k|k)\}_{i=0}^{N_{ss}} \leftarrow \{\hat{\boldsymbol{x}}_e^{(i)}(k|k)\}_{i=0}^{N_{ss}-1}$
20:     $\{\mathbf{P}^{(i)}(k|k)\}_{i=0}^{N_{ss}} \leftarrow \{\mathbf{P}_e^{(i)}(k|k)\}_{i=0}^{N_{ss}-1}$
21:     $N_{ss} \leftarrow N_{ss} - 1$
22:     **return** Fault with exclusion
23:   **else**
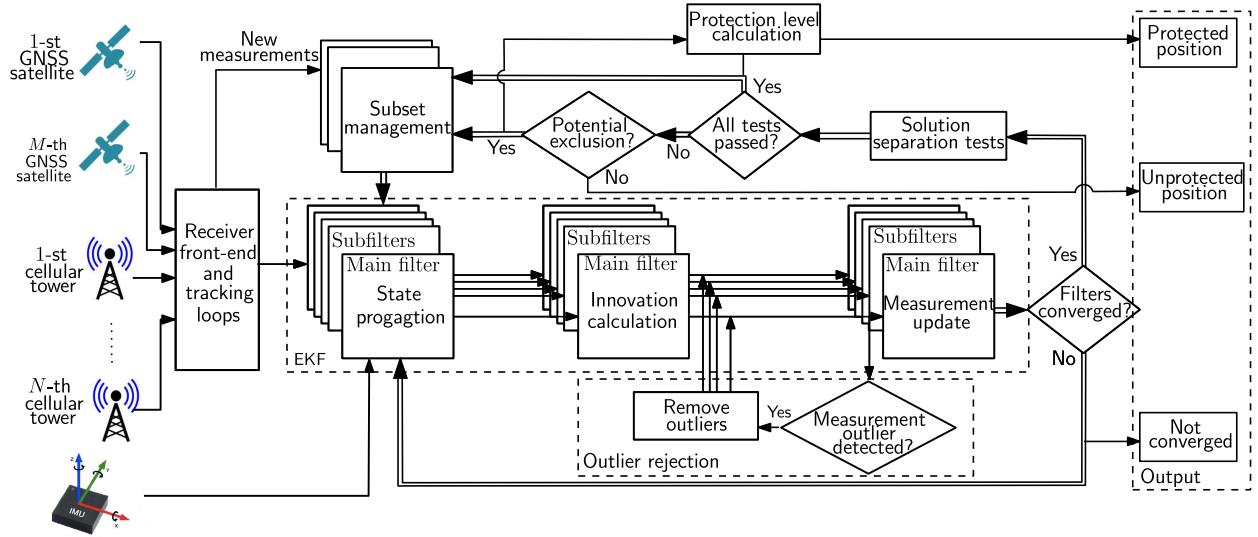24:   **return** No fault
25:   **end if**

Fig. 1. Solution separation RAIM for INS/GPS/SOP tightly-coupled navigation.

IV. Experimental Results

To demonstrate the proposed FDE framework and evaluate its performance under different sensor fusion scenarios, i.e., INS/GPS and INS/GPS/SOP, an experiment was conducted with a ground vehicle navigating in a suburban environment while collecting measurements from the on-board IMU, GPS, and two 5G gNBs.

A. Experimental Setup and RAIM Parameters

The experiment was conducted in Costa Mesa, California, USA. Two consumer-grade cellular omnidirectional Laird antennas were connected to a quadchannel National Instrument (NI) universal software radio peripheral (USRP)-2955 which was mounted on a ground vehicle. Two channels of the USRP was set up to sample 5G signals, which were processed by a software-defined radio (SDR) receiver to produce SOP pseudorange measurements. The vehicle was also equipped with a Septentrio AsteRx-i V integrated GNSS-IMU system to produce an RTK-corrected navigation solution, which are used as ground truth in this experiment. The raw IMU measurements and GPS pseudoranges from the Septentrio GNSS-IMU system are fed into the proposed framework to produce an INS/GPS/5G navigation solution and support FDE.

During the experiment, the ground vehicle was able to track 9 GPS satellites and receive 5G signals from 2 ambient gNB towers. The experiment environment and 5G tower locations are shown in Fig. 2.

The integrity risk budget. i.e., probability of hazardous misleading information (PHMI), are set to be 10^{-4}/h. The probability of false alert is targeted at 10^{-3}/h. The probability of fault for both GPS and 5G towers is set to be 10^{-2}/h and the time of influence for each fault is set to be 120 s . Considering the measurement rate in this experiment is 5 Hz yields RAIM parameters in the notation of per point as shown in Table I.

TABLE I
RAIM PARAMETERS

Parameter	Definition	Value
$\{\sigma_{\text{URA},m}^{\text{GPS}}\}_{m=1}^{M}$	User Range Error for GPS	5 m
$\{\sigma_{\text{URA},n}^{\text{S}}\}_{n=1}^{N}$	User Range Error for SOP	5.48 m
$PHMI_{\text{HOR}}$	Integrity budget for the horizontal component	1.1×10^{-9}
$PHMI_{\text{VERT}}$	Integrity budget for the vertical component	1.1^{-11}
$P_{\text{fa,HOR}}$	Continuity budget allocated to the vertical component	5.6×10^{-8}
$P_{\text{fa,VERT}}$	Continuity budget allocated to the vertical component	5.6×10^{-10}
$\{P_{\text{GPS}_m}\}_{m=1}^{M}$	Probability of a single GPS satellite fault	5.6×10^{-7}
$\{P_{\text{SOP}_n}\}_{n=1}^{N}$	Probability of a single SOP fault	5.6×10^{-7}

B. Experimental Results

Since the experiment was conducted in a suburban environment, which was not as challenging for GPS and 5G signals, and the GPS and 5G pseudorange measurements were produced by advanced receivers, no faults appeared in the pseudoranges. To mimic GPS faults, it was hypothesized that the ionospheric and troposhperic errors for the GPS satellite with PRN 7 were not properly corrected, which caused ranging errors with an average magnitude of 4.57 m.

The ground vehicle traversed a trajectory of 1.91 km in 200 seconds. The proposed framework was first implemented by fusing INS and GPS measurements. As shown in Fig. 3, the test statistic of INS/GPS did not surpass the test threshold, which indicates that the system failed to detect the hypothesized fault in the GPS satellite. However, in the case where two 5G towers were fused, the test statistic increased and test threshold decreased to a level that the system could detect the GPS fault.
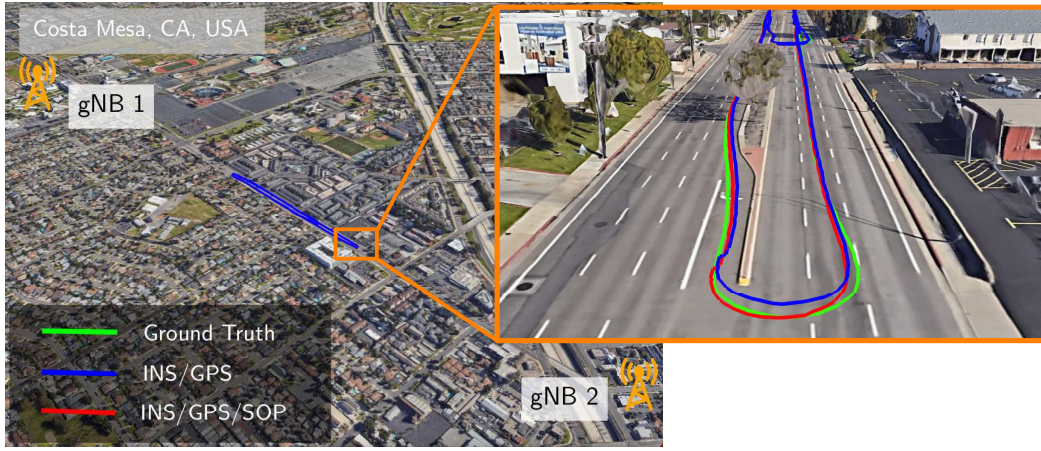
Fig. 2. Experiment layout, ground-truth trajectory (green), and navigation solutions with hypothesized fault GPS measurements: INS/GPS (blue) and INS/GPS/5G (red).

After the fault got excluded by the FDE algorithm described in Section III-C, the INS/GPS/5G achieved a position RMSE of 0.81 m and maximum position error of 2.17 m. The undetected GPS fault increased the RMSE and maximum position error to 1.83 m and 4.25 m, respectively, as summarized in Table II.
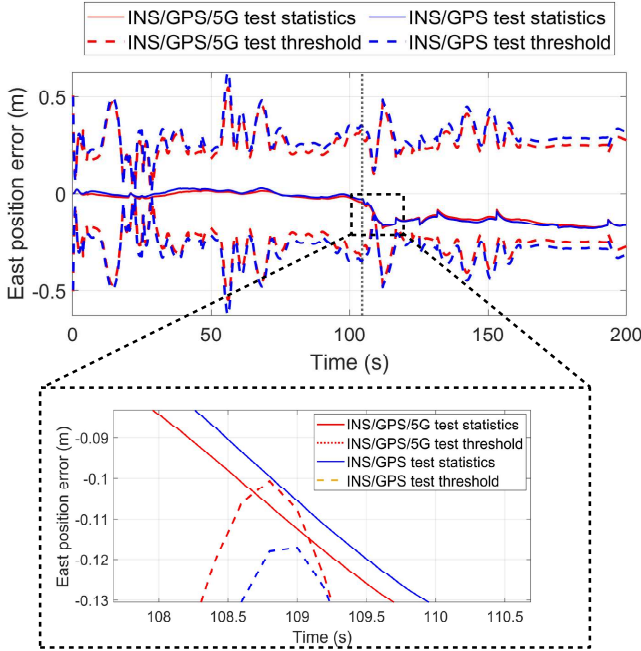

Fig. 3. Test statistics (solid) and test thresholds (dashed) for INS/GPS (blue) and INS/GPS/5G (red)

TABLE II
PERFORMANCE COMPARISON BETWEEN INS/GPS AND INS/GPS/5G

	INS/GPS	INS/GPS/SOP
RMSE (m)	1.8309	0.8116
Maximum error (m)	4.2505	2.1686

V. CONCLUSION

This paper developed a solution separation-based RAIM framework for INS/GPS/SOP tightly-coupled navigation systems. This framework conducts solution separation tests to instantaneously detect and exclude ranging measurement faults from GPS and SOP. The FDE performance of the proposed framework was validated experimentally, where 5G signals were exploited to improve FDE over fusing INS only with GPS signals. It was shown that fusing 5G enables the system to detect a fault from GPS satellites, which fusing only INS and GPS fails to detect. With the faulty measurements detected and excluded, INS/GPS/5G achieved a position RMSE of 0.81 m, while INS/GPS yielded a RMSE of 1.83 m. The FDE also reduced the maximum error from 4.25 m to 2.17 m.

REFERENCES

[1] H. Jing, Y. Gao, S. Shahbeigi, and M. Dianati, "Integrity monitoring of GNSS/INS based positioning systems for autonomous vehicles: State-of-the-art and open challenges," *IEEE Transactions on Intelligent Transportation Systems*, vol. 23, no. 9, pp. 14 166–14 187, 2022.

[2] N. Zhu, D. Betaille, J. Marais, and M. Berbineau, "GNSS integrity monitoring schemes for terrestrial applications in harsh signal environments," *IEEE Intelligent Transportation Systems Magazine*, vol. 12, no. 3, pp. 81–91, 2020.

[3] T. Reid, S. Houts, R. Cammarata, G. Mills, S. Agarwal, A. Vora, and G. Pandey, "Localization requirements for autonomous vehicles," *SAE International Journal of Connected and Automated Vehicles*, vol. 2, no. 3, pp. 173–190, September 2019.

[4] D. Imparato, A. El-Mowafy, and C. Rizos, "Integrity monitoring: From airborne to land applications," in *Multifunctional Operation and Application of GPS*. IntechOpen, 2018, pp. 23–43.

[5] T. Humphreys, M. Murrian, and L. Narula, "Deep-urban unaided precise global navigation satellite system vehicle positioning," *IEEE Intelligent Transportation Systems Magazine*, vol. 12, no. 3, pp. 109–122, 2020.

[6] K. Nagai, M. Spenko, R. Henderson, and B. Pervan, "Fault-free integrity and continuity for driverless urban vehicle navigation with multi-sensor integration: A case study in downtown Chicago," in *Proceedings of ION GNSS+ Conference*, September 2022, pp. 1350–1365.

[7] N. Souli, P. Kolios, and G. Ellinas, "Relative positioning of autonomous systems using signals of opportunity," in *Proceedings of IEEE Vehicular Technology Conference*, 2020, pp. 1–6.

[8] H. Dun, C. Tiberius, and G. Janssen, "Positioning in a multipath channel using OFDM signals with carrier phase tracking," *IEEE Access*, vol. 8, pp. 13 011–13 028, 2020.

[9] M. Pan, P. Liu, S. Liu, W. Qi, Y. Huang, X. You, X. Jia, and X. Li, "Efficient joint DOA and TOA estimation for indoor positioning with 5G picocell base stations," *IEEE Transactions on Instrumentation and Measurement*, vol. 71, pp. 1–19, 2022.

[10] Y. Wang, H. Zhu, T. Liang, and J. Qian, "Signals of opportunity navigation using LTE downlink signals," in *Proceedings of IEEE International Conference on Communication Technology*, September 2022, pp. 1070–1074.

[11] C. Jao, A. Abdallah, C. Chen, M. Seo, S. Kia, Z. Kassas, and A. Shkel, "PINDOC: Pedestrian indoor navigation system integrating deterministic, opportunistic, and cooperative functionalities," *IEEE Sensors Journal*, vol. 22, no. 14, pp. 14 424–14 435, July 2022.

[12] Z. Jiao, L. Chen, X. Lu, Z. Liu, X. Zhou, Y. Zhuang, and G. Guo, "Carrier phase ranging with DTMB signals for urban pedestrian localization and GNSS aiding," *Remote Sensing*, vol. 15, no. 2, pp. 423–446, 2023.

[13] X. Chen, Q. Wei, F. Wang, Z. Jun, S. Wu, and A. Men, "Super-resolution time of arrival estimation for a symbiotic FM radio data system," *IEEE Transactions on Broadcasting*, vol. 66, no. 4, pp. 847–856, December 2020.

[14] K. Strandjord, Y. Morton, and P. Wang, "Evaluating the urban signal environment for GNSS and LTE signals," in *Proceedings of ION GNSS+ Conference*, 2021, pp. 2166–2182.

[15] A. Abdallah and Z. Kassas, "Opportunistic navigation using sub-6 GHz 5G downlink signals: A case study on a ground vehicle," in *Proceedings of European Conference on Antennas and Propagation*, 2022, pp. 1–5.

[16] R. Whiton, J. Chen, T. Johansson, and F. Tufvesson, "Urban navigation with LTE using a large antenna array and machine learning," in *Proceedings of IEEE Vehicular Technology Conference*, 2022, pp. 1–5.

[17] C. Olone, H. Dhillon, and R. Buehrer, "Single-anchor localizability in 5G millimeter wave networks," *IEEE Wireless Communications Letters*, vol. 9, no. 1, pp. 65–69, 2020.

[18] A. Xhafa, J. del Peral-Rosado, J. López-Salcedo, and G. Seco-Granados, "Evaluation of 5G positioning performance based on UTDoA, AoA and base-station selective exclusion," *Sensors*, vol. 22, no. 1, pp. 101–118, 2021.

[19] A. Abdallah, J. Khalife, and Z. Kassas, "Experimental characterization of received 5G signals carrier-to-noise ratio in indoor and urban environments," in *Proceedings of IEEE Vehicular Technology Conference*, April 2021, pp. 1–5.

[20] I. Lapin, G. Granados, J. Samson, O. Renaudin, F. Zanier, and L. Ries, "STARE: Real-time software receiver for LTE and 5G NR positioning and signal monitoring," in *Proceedings of Workshop on Satellite Navigation Technology*, April 2022, pp. 1–11.

[21] J. del Peral-Rosado, P. Nolle, F. Rothmaier, S. Razavi, G. Lindmark, X. Jiang, D. Shrestha, F. Gunnarsson, S. Parsawar, R. Mundlamuri, F. Kaltenberger, N. Sirola, O. Sarkka, U. Noman, J. Rostrom, K. Vaarala, P. Miettinen, S. Garlaschi, L. Canzian, H. Babaroglu, E. Rastorgueva-Foi, M. Turunen, J. Talvitie, and D. Flachs, "Proof-of-concept of dedicated aerial 5G and GNSS testbed for enhanced hybrid positioning," in *Proceedings of ION GNSS Conference*, September 2022, pp. 2362–2376.

[22] C. Jin, W. Tay, K. Zhao, K. V. Ling, and K. Sin, "A 5G/GNSS integrated positioning method," in *Proceedings of ION GNSS Conference*, September 2022, pp. 2429–2443.

[23] A. Abdallah and Z. Kassas, "UAV navigation with 5G carrier phase measurements," in *Proceedings of ION GNSS Conference*, September 2021, pp. 3294–3306.

[24] Z. Liu, L. Chen, X. Zhou, Z. Jiao, G. Guo, and R. Chen, "Machine learning for time-of-arrival estimation with 5G signals in indoor positioning," *IEEE Internet of Things Journal*, 2023, accepted.

[25] N. Zhu, J. Marais, D. Betaille, and M. Berbineau, "GNSS position integrity in urban environments: A review of literature," *IEEE Transactions on Intelligent Transportation Systems*, vol. 19, no. 9, pp. 2762–2778, September 2018.

[26] J. Blanch, T. Walter, P. Enge, S. Wallner, F. Amarillo Fernandez, R. Dellago, R. Ioannides, I. Fernandez Hernandez, B. Belabbas, A. Spletter *et al.*, "Critical elements for a multi-constellation advanced RAIM,"

[27] *NAVIGATION, Journal of the Institute of Navigation*, vol. 60, no. 1, pp. 53–69, 2013.

[27] A. Ene, J. Blanch, and T. Walter, "Galileo-GPS RAIM for vertical guidance," in *Proceedings of National Technical Meeting of The Institute of Navigation*, January 2006, pp. 18–20.

[28] T. Walter, J. Blanch, M. J. Choi, T. Reid, and P. Enge, "Incorporating GLONASS into aviation RAIM receivers," in *Proceedings of International Technical Meeting of the Institute of Navigation*, January 2013, pp. 239–249.

[29] Y. Liu, J. Zhang, R. Xue, and Z. Wang, "Performance analysis of advanced RAIM with the inclusion of BeiDou," in *Proceedings of ION International Technical Meeting*, 2014, pp. 3629–3636.

[30] P. Roysdon and J. Farrell, "GPS-INS outlier detection and elimination using a sliding window filter," in *Proceedings of American Control Conference*, May 2017, pp. 1244–1249.

[31] T. Li, L. Pei, Y. Xiang, Q. Wu, S. Xia, L. Tao, X. Guan, and W. Yu, "P3-LOAM: PPP/LiDAR loosely coupled SLAM with accurate covariance estimation and robust RAIM in urban canyon environment," *IEEE Sensors Journal*, vol. 21, no. 5, pp. 6660–6671, 2021.

[32] L. Fu, J. Zhang, R. Li, X. Cao, and J. Wang, "Vision-aided RAIM: A new method for GPS integrity monitoring in approach and landing phase," *Sensors*, vol. 15, no. 9, pp. 22 854–22 873, 2015.

[33] J. Xiong, J. Cheong, A. Dempster, and Z. Xiong, "An integrity monitoring method for multi-sensor collaborative navigation," in *Proceedings of IEEE/ION Position, Location, and Navigation Symposium*, April 2020, pp. 461–468.

[34] M. Maaref and Z. Kassas, "Measurement characterization and autonomous outlier detection and exclusion for ground vehicle navigation with cellular signals," *IEEE Transactions on Intelligent Vehicles*, vol. 5, no. 4, pp. 670–683, December 2020.

[35] M. Maaref and Z. Kassas, "Autonomous integrity monitoring for vehicular navigation with cellular signals of opportunity and an IMU," *IEEE Transactions on Intelligent Transportation Systems*, vol. 23, no. 6, pp. 5586–5601, June 2022.

[36] J. Khalife, M. Maaref, and Z. Kassas, "Opportunistic autonomous integrity monitoring for enhanced UAV safety," *IEEE Aerospace and Electronics Systems Magazine*, 2022, accepted.

[37] S. Hewitson and J. Wang, "Extended receiver autonomous integrity monitoring (eRAIM) for GNSS/INS integration," *Journal of Surveying Engineering*, vol. 136, no. 1, pp. 13–22, 2010.

[38] J. Blanch, T. Walter, L. Norman, K. Gunning, and L. de Groot, "Solution separation-based fd to mitigate the effects of local threats on ppp integrity," in *Proceedings of IEEE/ION Position, Location and Navigation Symposium*, April 2020, pp. 1085–1092.

[39] O. O. Crespillo, A. Grosch, J. Skaloud, and M. Meurer, "Innovation vs residual kf based GNSS/INS autonomous integrity monitoring in single fault scenario," in *Proceedings of ION GNSS+ Conference*, September 2017, pp. 2126–2136.

[40] C. Tanil, S. Khanafseh, M. Joerger, and B. Pervan, "Probabilistic data association techniques for target tracking with applications to sonar, radar and EO sensors," *IEEE Aerospace and Electronic Systems Magazine*, vol. 54, no. 1, pp. 131–143, 2018.

[41] M. Maaref, J. Khalife, and Z. Kassas, "Enhanced safety of autonomous driving by incorporating terrestrial signals of opportunity," in *Proceedings of IEEE International Conference on Acoustics, Speech and Signal Processing*, May 2020, pp. 9185–9189.

[42] M. Jia, J. Khalife, and Z. Kassas, "Evaluation of ground vehicle protection level reduction due to fusing GPS with faulty terrestrial signals of opportunity," in *Proceedings of ION International Technical Meeting*, January 2021, pp. 354–365.

[43] M. Jia and M. Kassas, "Kalman filter-based integrity monitoring for GNSS and 5G signals of opportunity integrated navigation," in *Proceedings of IFAC on Advances in Automotive Control*, vol. 55, August 2022, pp. 273–278.

[44] J. Morales and Z. Kassas, "Tightly-coupled inertial navigation system with signals of opportunity aiding," *IEEE Transactions on Aerospace and Electronic Systems*, vol. 57, no. 3, pp. 1930–1948, 2021.

[45] P. Groves, *Principles of GNSS, Inertial, and Multisensor Integrated Navigation Systems*, 2nd ed. Artech House, 2013.

[46] R. Young and G. McGraw, "Fault detection and exclusion using normalized solution separation and residual monitoring methods," *NAVIGATION, Journal of the Institute of Navigation*, vol. 50, no. 3, pp. 151–169, 2003.